HHS Public Access

Author manuscript

Contrast Media Mol Imaging. Author manuscript; available in PMC 2017 September 01.

Published in final edited form as:

Contrast Media Mol Imaging. 2016 September ; 11(5): 371–380. doi:10.1002/cmmi.1701.

Uptake and retention of manganese contrast agents for PET and MRI in the rodent brain

Christina L Brunnquell[1], **Reinier Hernandez**[1], **Stephen A Graves**[1], **Ivy Smit-Oistad**[2], **Robert J Nickles**[1], **Weibo Cai**[1,3], **M Elizabeth Meyerand**[1,4,*], and **Masatoshi Suzuki**[2,4,*]

[1]Department of Medical Physics, University of Wisconsin – Madison, Madison, WI, USA

[2]Department of Comparative Biosciences, University of Wisconsin – Madison, Madison, WI, USA

[3]Department of Radiology, University of Wisconsin – Madison, Madison, WI, USA

[4]Department of Biomedical Engineering, University of Wisconsin – Madison, Madison, WI, USA

Abstract

Manganese-enhanced magnetic resonance imaging (MRI) is an established neuroimaging method for signal enhancement, tract tracing, and functional studies in rodents. Along with the increasing availability of combined positron emission tomography (PET) and MRI scanners, the recent development of the positron-emitting isotope ^{52}Mn has prompted interest in the use of Mn^{2+} as a dual-modality contrast agent. In this work, we characterized and compared the uptake of systemically delivered Mn^{2+} and radioactive $^{52}Mn^{2+}$ in the rat brain for MRI and PET, respectively. Additionally, we examined the biodistribution of two formulations of $^{52}Mn^{2+}$ in the rat. In MRI, maximum uptake was observed one day following delivery of the highest $MnCl_2$ dose tested (60 mg/kg), with some brain regions showing delayed maximum enhancement 2–4 days following delivery. In PET, we observed low brain uptake after systemic delivery, with a maximum of approximately 0.2 %ID/g. We also studied the effect of final formulation vehicle (saline compared to $MnCl_2$) on $^{52}Mn^{2+}$ organ biodistribution and brain uptake. We observed that the addition of bulk Mn^{2+} carrier to $^{52}Mn^{2+}$ in solution resulted in significantly reduced $^{52}Mn^{2+}$ uptake in the majority of organs, including the brain. These results lay the groundwork for further development of ^{52}Mn PET or dual Mn-enhanced PET/MR neuroimaging in rodents and indicate several interesting potential applications of ^{52}Mn PET in other organs and systems.

Keywords

manganese-enhanced magnetic resonance imaging (MEMRI, MRI); positron emission tomography (PET); manganese; quantitative imaging; neuroimaging

[*]Corresponding author information: Masatoshi Suzuki, Ph.D., D.V.M., Address: 4124 Veterinary Medicine Building, 2015 Linden Drive, Madison, WI 53706, Tel: (608) 262-4264, Fax: (608) 890-3667, masatoshi.suzuki@wisc.edu. M. Elizabeth Meyerand, Ph.D., Address: 1129 Wisconsin Institutes for Medical Research, 1111 Highland Ave, Madison, WI 53705, Tel: (608) 263-1685, Fax: (608) 265-9840, memeyerand@wisc.edu.

1. Introduction

The T_1-weighted signal-enhancing MRI contrast agent manganese (Mn^{2+}) has been studied and applied in preclinical animal models and human subjects for imaging liver disease, cancer, cardiac viability, and brain function and structure (1–4). To avoid the toxic effects of this metal when using the large doses required for MR signal enhancement, only the chelated form Mn-DPDP (Magnafodipir, Teslascan®) and an oral $MnCl_2$ agent (LumenHance®) have been approved for use in human patients (5). Because unchelated Mn^{2+} can be transported via Ca^{2+} channels, uptake and resulting T_1 enhancement can indicate function and highlight structure in the heart and brain. Therefore, it has been applied in a variety of preclinical functional imaging studies, primarily in rodents (6–8). Mn^{2+} enhancement in the myocardium reflects viability, while uptake in the brain can reflect functional activation, connected neuronal tracts, or can be used for general tissue enhancement and cytoarchitecture visualization (7, 9). $MnCl_2$ biodistribution studies in rats have also indicated high uptake of Mn^{2+} in a variety of other organs and glands including the liver, kidney, salivary glands, and pancreas (10).

Recently, the positron-emitting isotope ^{52}Mn ($t_{1/2}$ = 5.59 days) has been produced for PET imaging by several groups, including our own (11–16). Two factors have played a role in recent development of ^{52}Mn as a PET contrast agent: first, the general interest in and investigation of longer-lived radiometals for antibody-based PET imaging (17, 18), and second, the development of simultaneous PET/MRI systems (19), with $^{52}Mn^{2+}$ having potential as a dual-modality signal-enhancing contrast agent. Because PET imaging typically requires tracer doses, the availability of ^{52}Mn could facilitate the clinical investigation and application of Mn^{2+}-based imaging of function and viability that have been developed in preclinical models with manganese-enhanced MRI (MEMRI).

In the setting of neuroimaging, methods for MEMRI in the rodent have been developed for a variety of applications, including generalized cytoarchitecture enhancement, activation studies, and neuronal tract tracing (2, 9). Along with determining the best way to deliver Mn^{2+} for appropriate brain uptake and enhancement, several methods have already been proposed to minimize toxicity while delivering the maximum dose possible for sufficient imaging contrast (9, 20). For instance, intrathecal injection and osmotic pumps are intriguing alternative methods for Mn^{2+} administration (21, 22). Several other works also assert that slow systemic delivery via tail vein infusion can sufficiently reduce toxicity without the need for more specialized delivery techniques (23, 24). Specifically, one such study examined the effect of varying the time between contrast administration and imaging, and confirmed a correlation between R_1 relaxation rate ($R_1=1/T_1$) and *ex vivo* elemental analysis of Mn uptake (24). This work showed maximum T_1 change at one day following contrast administration, but did not address slightly later time points between 2–4 days, which are of interest to further reduce the potential combined effects of Mn^{2+} and isoflurane (for imaging anesthesia) on animal health. An additional motivation in our laboratory is related to the uptake of Mn^{2+} in specific brain regions, such as the striatum, for imaging grafted stem cells (12).

Compared to MEMRI, ^{52}Mn PET has been much less thoroughly investigated in terms of contrast agent delivery, ^{52}Mn biodistribution, PET image acquisition, and image reconstruction and analysis techniques. Few published studies address ^{52}Mn PET, with the majority of these works focusing on production and separation of the isotope rather than *in vivo* imaging applications (11, 14, 15). As demonstrated by Topping and colleagues (11) and confirmed in our recent studies (12), relatively low brain uptake of $^{52}Mn^{2+}$ (less than 0.5% ID/g) is observed *in vivo*. To improve brain uptake, $^{52}Mn^{2+}$ supplementation with bulk $MnCl_2$ may potentially increase circulation time and therefore allow more $^{52}Mn^{2+}$ to be transported or diffuse into the brain, both of which are mechanisms of brain Mn^{2+} uptake (11, 25–28). The supplementation of $^{52}Mn^{2+}$ with $MnCl_2$ could also be of interest for simultaneous PET/MRI studies, further prompting more thorough investigation of this contrast agent preparation.

In this study, we characterize and directly compare the uptake of $^{52}Mn^{2+}$ and non-radioactive Mn^{2+} in the rat brain using MRI and PET imaging, using similar contrast delivery and image time course protocols for both modalities. With these experiments, we aim to provide new knowledge regarding the contrast agent composition, dose, delivery method, and imaging time point to maximize contrast enhancement and ^{52}Mn detectability in the rat brain. By testing the uptake and biodistribution characteristics of both no-carrier-added (NCA) and carrier-added (CA) $^{52}Mn^{2+}$, we further hope to elucidate whether Mn^{2+} could be used as a dual-modality signal-enhancing contrast agent for PET/MR of the brain as well as other organs or systems of interest. For our further pursuit of manganese-based imaging of transplanted stem cells (12), the goal of these studies is to select the best contrast agent dose, formulation, delivery method, and imaging time point to facilitate sufficient Mn^{2+} supplementation for uptake and detection of cells over-expressing a Mn^{2+} transporter protein.

2. Results

2.1. Brain uptake and efflux measured by MEMRI

To observe the effect of $MnCl_2$ dose and imaging time point on signal enhancement in the brain, we administered three doses of $MnCl_2$ to rats (30, 45, and 60 mg/kg, N=3 per dose group) using slow i.v. infusion as described above. We then performed T_1 mapping with MRI over the course of two weeks following $MnCl_2$ administration. R_1 relaxation rate ($R_1 = 1/T_1$) in the whole brain and in specific brain sub-regions was estimated from a set of variable flip angle spoiled gradient echo (SPGR) acquisitions at each time point.

After T_1 mapping and manual segmentation, whole-brain R_1 enhancement was measured at all time points and doses. Representative R_1 maps in a single subject for each dose group over the course of 2 weeks are shown in Fig. 1 and Supplementary Fig. 1. General T_1 shortening was observed in the whole brain, with greatest enhancement near the ventricles and diffusing throughout neighboring regions over time. The greatest whole-brain R_1 enhancement was observed one day following contrast administration for all doses tested (Fig. 2A). Due to a high level of inter-subject variability of uptake, significant differences were not observed between dose groups, although there was a clear trend toward increased

signal enhancement in the rats from the higher dose groups compared to the 30 mg/kg dose group (Figs. 1 and 2A).

Quantification of R_1 relaxation rate in specific brain regions was performed via manual segmentation of the brain prior to registration to a Sprague Dawley rat brain atlas for regional delineation. We then determined R_1 enhancement in the striatum, relevant for our stem cell imaging work, along with a variety of other brain regions of interest. Median R_1 rates were determined in the striatum, neocortex, olfactory bulb, corpus callosum, basal forebrain, globus pallidus, thalamus, hippocampus, hypothalamus, brain stem, cerebellum, and trigeminal tract. The maximum R_1 relaxation rate measured in each region for each dose level is shown in Table 1. Some regions, such as the neocortex, corpus callosum, basal forebrain, hippocampus, hypothalamus, and cerebellum, consistently reached maximum signal one day following contrast administration (Table 1 and Fig. 2). Other regions, in particular the striatum, globus pallidus, thalamus, and brain stem, reached their maximum signal level at either 1, 2, or 4 days following contrast administration, depending on dose delivered. Together, these results indicate that up to 60 mg/kg $MnCl_2$ can be delivered for brain imaging between 1–4 days following contrast administration, depending on the enhancement level and brain structure(s) of interest.

2.2. Brain uptake of $^{52}Mn^{2+}$ measured by gamma counting

To observe brain uptake of no-carrier-added (NCA, formulated in saline) and carrier-added (CA, formulated in 66.7 mM $MnCl_2$ in saline) $^{52}Mn^{2+}$, gamma counting was performed on resected rat brains at 24 and 48 hours following contrast agent administration (N=3 per group, Figure 3B). Significant increases in $^{52}Mn^{2+}$ brain uptake were observed in subjects delivered NCA $^{52}Mn^{2+}$ compared to those delivered CA $^{52}Mn^{2+}$, by a factor of greater than 2.5 at both time points evaluated (Fig. 3A and B, $p<0.01$). Additionally, a trend toward approximately 30% increased uptake at 48 hours compared to 24 hours was observed for both contrast agent forms. The results of gamma counting indicate that significantly higher brain uptake of $^{52}Mn^{2+}$ is observed when administered in no-carrier-added form.

2.3. In vivo brain uptake of ^{52}Mn

In vivo full-body PET/CT was performed in six rats at various time points following administration of CA $^{52}Mn^{2+}$ (N=1) and NCA $^{52}Mn^{2+}$ (N=5). In order to examine brain uptake dynamics of the two formulations of $^{52}Mn^{2+}$, ROI-based analysis on full-body PET images was used to compare brain uptake between two subjects delivered CA and NCA $^{52}Mn^{2+}$, respectively, at multiple time points up to 7 days following administration. PET acquisition times ranged from 30–60 minutes due to the relatively long half-life of ^{52}Mn ($t_{1/2}$=5.59 days). In the subject delivered CA $^{52}Mn^{2+}$, brain uptake between 0.08–0.10 %ID/g was observed, with maximum uptake measured at the earliest time point (24 hours) post injection (Fig. 3C). As expected, in the subject delivered NCA $^{52}Mn^{2+}$, higher brain uptake of 0.10–0.16 %ID/g was observed. Surprisingly, the maximum brain uptake was measured at 2 hours following contrast administration, rather than at 48 hours, as gamma-counting results would suggest. Notably, we observed several regions of high $^{52}Mn^{2+}$ uptake in the head and neck, including the pituitary and the submandibular glands (Fig. 4A).

After observing maximum uptake of NCA $^{52}Mn^{2+}$ at the 2 hour imaging time point, we further investigated the uptake dynamics of NCA $^{52}Mn^{2+}$ in four additional subjects (Fig. 4). PET/CT images were acquired at multiple time points over the course of 8 hours and at 24, 48, and 72 hours (N=3 at 72 hour time point) following contrast administration. In these subjects, ROI-based time activity curves indicated uptake of $^{52}Mn^{2+}$ in the first hour followed by a steady, slow decrease in retention over the course of 3 days (Fig. 4A and B). In order to understand the source of the discrepancy between brain uptake dynamics with gamma counting and PET/CT imaging, ROI-based analysis of submandibular glands and pituitary uptake was also performed on all subjects. Due to high uptake in these regions, signal spillover could affect quantification of adjacent brain uptake measurements (Fig. 4A). The submandibular glands exhibited uptake over the course of 4 hours, reaching maximum uptake of 0.869 %ID/g at 4 hours following contrast administration and followed by a slow decrease over the next 72 hours (Fig. 4C). Similarly, the pituitary showed maximum uptake at 4 hours, reaching 0.512 %ID/g. These signal levels correspond to 5.3 and 3.1 times the whole-brain average uptake at that time point, respectively. Together, these results indicate that although maximum brain uptake of ^{52}Mn is measured in PET/CT 1–4 hours following administration, measurements may be skewed to higher than ground truth due to spillover effects from nearby high signal regions.

2.4. ^{52}Mn full-body biodistribution

Due to the extensive application of $MnCl_2$ as an MRI contrast agent in recent decades, the biodistribution of Mn^{2+} for rodent MRI has been previously investigated (10). However, the biodistribution and organ uptake of NCA and CA ^{52}Mn has not yet been established in the literature. Therefore, in order to more thoroughly characterize this new PET agent prior to application for imaging tasks, e*x vivo* measurements of NCA and CA $^{52}Mn^{2+}$ uptake in major organs were made at 4 and 48 hours following contrast delivery (Fig. 5A). At four hours following ^{52}Mn delivery, the highest uptake of NCA $^{52}Mn^{2+}$ was observed in the kidney (3.02 %ID/g), liver (2.75 %ID/g), pancreas (1.74 %ID/g), stomach (1.50 %ID/g), and submandibular gland (1.36 %ID/g). Interestingly, unlike in other organs, high pancreas and submandibular gland uptake was maintained at the 48-hour time point (2.49 and 1.24 %ID/g, respectively). Intestine uptake also remained relatively consistent from 4 to 48 hours following delivery (1.00 and 0.75 %ID/g, respectively). After CA $^{52}Mn^{2+}$ delivery, the highest uptake was observed in the pancreas (1.94 %ID/g), which had approximately 2.5 times higher uptake than the next highest uptake observed in the submandibular gland (0.79 %ID/g). The uptake of CA $^{52}Mn^{2+}$ was significantly reduced compared to the uptake of NCA $^{52}Mn^{2+}$ at both time points in all organs tested with the exception of the bone, tail, blood, pancreas (significant difference at 4 hour time point only), and intestine (significant difference at 48 hour time point only) ($p<0.05$).

Qualitative observations of CA and NCA $^{52}Mn^{2+}$ biodistribution with *in vivo* PET/CT generally agreed with *ex vivo* biodistribution studies (Fig. 5B). At 24 hours following NCA $^{52}Mn^{2+}$ delivery, high uptake was observed in the liver, kidneys, salivary glands, gastrointestinal tract, pancreas, and spleen. At the same time point following CA $^{52}Mn^{2+}$ delivery, uptake was primarily observed in the contents of the intestinal tract and cecum as well as in the vicinity of intervertebral and synovial joints (Fig. 5C). Signal persisted in the

gastrointestinal tract (NCA) and joints (CA) at later imaging time points (data not shown). Increased uptake of CA $^{52}Mn^{2+}$ compared to NCA $^{52}Mn^{2+}$ was observed in synovial and intervertebral joints at all *in vivo* imaging time points. In all subjects imaged with full-body PET/CT, we observed activity pooling in the tail at the injection site to varying degrees. This was possibly caused by movement of the injection needle during the slow infusion, which lasted between 15–45 minutes depending on bulk $MnCl_2$ dose, and could be a contributor to the inter-subject variability of uptake measurements observed *in vivo*.

3. Discussion

In this work, we investigated the effects of contrast agent vehicle, dose, and acquisition time point on brain uptake and retention of Mn^{2+}-based contrast agents for MRI and PET. The bulk doses of Mn^{2+} systemically delivered for MEMRI in the rodent brain are known to cause somnolence as well as side effects in the liver, heart, and brain (29, 30). By using a bulk $MnCl_2$ delivery protocol that utilized slow infusion while maintaining body temperature and hydration, we observed minimal behavior and health side effects, even at the highest dose tested (60 mg/kg). Although we observed lethargy in rats immediately after delivery and recovery from anesthesia, all subjects recovered to normal demeanor and activity levels in less than 24 hours. Our observations support the methods used by other labs in rats, in which even higher total doses of 110–175 mg/kg $MnCl_2$ were delivered (24, 31). In all measurements of Mn uptake in this work, inter-subject variability was observed. With whole-body PET/CT, we noted activity pooled in the tail, most likely caused by the needle moving slightly during the slow 15–45 minute infusion of contrast agent. This likely occurred in all subjects to some extent, not just those imaged with PET/CT, and therefore could be one source of inter-subject variability of brain uptake dynamics (along with normal biological and physiological variations). For gamma counting and PET/CT studies that require trace amounts of $^{52}Mn^{2+}$, rather than large doses of bulk $MnCl_2$, a faster infusion of NCA $^{52}Mn^{2+}$ would likely be advisable. We hypothesize that this would minimize errors with needle placement, reducing the Mn^{2+} delivered to the tail rather than the blood pool and minimizing variability between subjects.

In MRI studies, we observed that greater $MnCl_2$ dose resulted in increased R_1 enhancement, in the whole brain and in a variety of individually analyzed brain regions. This maximum enhancement occurred at one day following contrast administration for the whole brain on average as well as for a majority of brain regions. The delayed maximum enhancement observed in some regions, most notably the striatum, thalamus, globus pallidus, and brain stem, may be a result of more prolonged uptake over greater than 24 hours and/or slower Mn^{2+} efflux from these brain regions. This indicates that neuroimaging studies focused on these regions may perform favorably at these later time points due to both increased enhancement and reduced combined negative effects of bulk $MnCl_2$ administration and isoflurane anesthesia for imaging on study subjects.

The spatial pattern of R_1 enhancement observed was characterized by a small amount of generalized enhancement with increased enhancement near the ventricles. This pattern agreed with other studies that show saturable active transport of Mn^{2+} to the brain parenchyma across the BBB with additional uptake via diffusion through the blood-CSF

barrier, linearly correlated with the blood concentration of Mn^{2+} (25–29). Furthermore, we observed slow reduction of Mn^{2+} enhancement in the brain, consistent with previous studies establishing diffusion as the primary efflux mechanism (29, 32).

In gamma counting studies we observed that supplementing $^{52}Mn^{2+}$ with bulk $MnCl_2$ (CA $^{52}Mn^{2+}$) resulted in reduced brain uptake by an average factor of greater than two. This is most likely due to competition between cold Mn^{2+} and $^{52}Mn^{2+}$ for Mn^{2+} transporters into the brain (26, 29). At both 4 and 48 hours following contrast delivery, *ex vivo* biodistribution studies showed low plasma activity (<0.025 %ID/g) independent of contrast agent dose. These results indicate that, at the contrast doses and measurement times used for biodistribution studies in this work, adding bulk $MnCl_2$ to $^{52}Mn^{2+}$ prior to delivery does not significantly increase $^{52}Mn^{2+}$ circulation time, which was previously hypothesized as a potential method to increase overall ^{52}Mn brain uptake (11).

Regarding the timing window of maximum $^{52}Mn^{2+}$ uptake in the brain, there was a disagreement between *ex vivo* gamma counting and *in vivo* PET imaging. Gamma counting experiments of the excised brain indicated a non-significant increase in brain activity from 24 to 48 hours, while ROI-based analysis of *in vivo* PET/CT indicated maximum brain uptake within the first eight hours. Based on imaging studies in six subjects, we observed maximum brain uptake 1–4 hours following NCA $^{52}Mn^{2+}$ administration. However, the ROI-based brain uptake measurements may be artificially high due to spillover from nearby high-signal regions such as the submandibular glands and pituitary. An additional source of timing discrepancy may be the inter-subject variability of ^{52}Mn delivery, which could affect the dynamics of ^{52}Mn brain uptake through saturable transporters or the blood-CSF barrier. Nevertheless, this maximum uptake of approximately 0.2% ID/g may be too low for many $^{52}Mn^{2+}$ neuroimaging applications, and alternate delivery methods such as blood-brain-barrier disruption or direct CSF delivery of $^{52}Mn^{2+}$ may be worthy of future investigation. In studies in which an accumulation of $^{52}Mn^{2+}$ is expected in a specific brain region of interest, such as for stem cell tracking, systemic delivery may prove sufficient when the appropriate formulation and imaging time point are utilized (12).

Systematic studies of ^{52}Mn biodistribution in the rat, which have not previously been described in the literature, indicate patterns of retention and uptake that may be of interest for imaging applications outside the central nervous system. Although biodistribution studies were not the intended emphasis of this work, the interesting results warrant further discussion and investigation. We observed that the preparation of $^{52}Mn^{2+}$ in $MnCl_2$ solution caused reduced uptake in the majority of organs as well as kidney and liver excretion of much of the injected activity over the course of 4–48 hours following administration. Interestingly, full-body PET/CT after administration of CA $^{52}Mn^{2+}$ showed uptake in intervertebral and synovial joints. Although this work does not focus on musculoskeletal applications of ^{52}Mn PET, this uptake pattern may be of interest to other preclinical imaging researchers and warrants further investigation. Because Mn is an important osteotropic element, irregularity or change in ^{52}Mn uptake in joints and bone may be indicative of underlying skeletal deficiencies or of response to treatment thereof, respectively (33).

In both CA and NCA preparations, ^{52}Mn uptake greater than 0.5 %ID/g was observed in the liver, kidney, pancreas, and salivary glands. These results are in qualitative agreement with reports in the literature of Mn^{2+} biodistribution studies after non-radioactive $MnCl_2$ administration (10). Interestingly, uptake in the pancreas and salivary glands was maintained until the later 48 hour time point after delivery of NCA $^{52}Mn^{2+}$. We hypothesize that the long-term retention of $^{52}Mn^{2+}$ in the pancreas and salivary glands, particularly following delivery of NCA $^{52}Mn^{2+}$, may be attributable to the higher endogenous levels of manganese present in glandular organs such as these (10). Exchange between the endogenous and exogenous pools of Mn^{2+} following NCA $^{52}Mn^{2+}$ administration would result in mitochondrial localization and sequestration (34). In the case of CA $^{52}Mn^{2+}$, uptake may not be sustained for as long for several reasons. Because the secretory cells of the pancreas and salivary glands have mechanisms for Ca^{2+} efflux to maintain homeostasis, the higher levels of Mn^{2+} accumulating in the cell cytoplasm following CA $^{52}Mn^{2+}$ delivery may exit the cells via this same pathway (35, 36). Furthermore, radiolabeled Mn^{2+} efflux may be stimulated by high extracellular Mn^{2+} concentrations, as has been observed in cultured rat astrocytes (37). This $^{52}Mn^{2+}$ efflux would likely be far less dramatic following delivery of trace $^{52}Mn^{2+}$ levels in the NCA formulation, resulting in greater retention of $^{52}Mn^{2+}$ in the cell.

MR imaging in the majority of the organs in which high $^{52}Mn^{2+}$ uptake was observed has previously been pursued experimentally and in clinical imaging settings (38–40). For diagnostic purposes, $^{52}Mn^{2+}$ uptake may be reflective of acinar cell function in both the pancreas and salivary glands and β–cell function in the pancreas (38, 39). Particularly in NCA formulation, ^{52}Mn uptake in the pancreas and salivary glands may increase the potential for PET-based diagnosis or disease monitoring, as much lower contrast doses would be required for PET than for $MnCl_2$-enhanced MR studies. Furthermore, a shorter-lived isotope of manganese without confounding gamma emissions, ^{52}Mn ($t_{1/2}$ = 46 min, β^+ = 97%) can also be produced on low-energy medical cyclotrons by the ^{50}Cr(d,n) and ^{54}Fe(p,α) reactions. The production of this isotope is currently underway at our institution, which may lead to greater clinical translatability of NCA Mn-based PET imaging.

4. Conclusions

MEMRI has been established as a useful preclinical neuroimaging method for observing brain tissue enhancement, neuron tract tracing, functional imaging, and stem cell detection. However, the doses required for T_1-weighted signal enhancement are prohibitive for translation of these applications. Heightened interest in ^{52}Mn PET imaging has resulted in its investigation as a novel imaging method with potential for reduced bulk Mn^{2+} dose, complementary imaging characteristics, and applications in simultaneous PET/MR. In these studies we have investigated several methods for preparation, delivery, and detection of Mn^{2+}-based contrast agents with quantitative MEMRI and ^{52}Mn PET. We observed that while the whole brain and many brain regions reach maximum R_1 in MEMRI at 24 hours following $MnCl_2$ delivery, several specific sub-regions show maximum enhancement at later time points. However, at the tracer doses of $^{52}Mn^{2+}$ delivered for PET imaging, brain uptake was insufficient for practical application in most neuroimaging studies (in the case of an

intact blood-brain barrier). With PET/CT and *ex vivo* gamma counting, we observed that the supplementation of tracer doses of ^{52}Mn with $MnCl_2$ reduced activity uptake in the brain and nearly all other organs. For this reason, along with the reduced bulk Mn^{2+} dose, NCA $^{52}Mn^{2+}$ holds greater potential as the preferable contrast agent form for imaging applications. Despite a lack of promise in our $^{52}Mn^{2+}$ neuroimaging results, these studies highlight several interesting areas of further study of ^{52}Mn PET, including investigating specific $^{52}Mn^{2+}$ uptake in the salivary glands, pancreas, and joints. In the future, additional development of methods to increase $^{52}Mn^{2+}$ uptake in the brain could be of great interest.

5. Experimental

5.1. Animal experimentation

All animal experimentation was performed following NIH guidelines and in accordance with protocols approved by the University of Wisconsin Institutional Animal Care and Use Committee. Adult female Sprague Dawley rats were used for experiments. Rats were housed under controlled temperature and light conditions and had free access to food and water. Upon completion of experimentation, rats were euthanized by slowly introducing CO_2 to the rat in an enclosed chamber.

5.2. Systemic delivery of Mn

In preparation for imaging, rats were delivered Mn^{2+} in the form of $MnCl_2$ and/or $^{52}Mn^{2+}$ in solution. Animals were anesthetized with light isoflurane (0.5–2% in oxygen) and placed on a warming pad to maintain body temperature. Contrast agent, prepared as described below, was delivered via tail vein with an infusion pump at a rate of 2 mL/hr. Following infusion, the infusion line was flushed with heparinized saline and animals were delivered 5 mL pre-warmed saline subcutaneously.

Prior to MRI, doses of 30, 45, and 60 mg/kg $MnCl_2$ at a concentration of 66.7 mM in bicine-buffered saline were delivered to 9 animals (N=3 per group). ^{52}Mn was prepared as described previously, with an average specific activity of 0.8 GBq/μmol (13). No-carrier-added (NCA) $^{52}Mn^{2+}$ was prepared by diluting $^{52}Mn^{2+}$ in saline to 1.5 mCi/mL (55.5 MBq/mL) then delivered at a dose of 2 mCi/kg (74 MBq/kg, N=6 for *ex vivo* gamma counting and N=4 for *in vivo* PET/CT). Alternatively, $^{52}Mn^{2+}$ was diluted in 66.7 mM buffered $MnCl_2$ solution at a concentration of 0.37 mCi/mL (13.7 MBq/mL). In this preparation, animals were delivered 2 mCi/kg (74 MBq/kg) $^{52}Mn^{2+}$ in approximately 45 mg/kg $MnCl_2$, which corresponds to the average dose used for MEMRI studies (N=6 for *ex vivo* gamma counting and N=1 for *in vivo* PET/CT). This contrast agent preparation is herein referred to as carrier-added (CA) $^{52}Mn^{2+}$.

5.3. MEMRI

To observe brain Mn^{2+} uptake with MRI, *in vivo* R_1 mapping was performed using a 4.7 T preclinical MRI scanner (Agilent Technologies, Santa Clara, CA, USA). At each imaging time point, a series of 3D SPGR images were acquired using the following pulse sequence parameters: TR = 5.96 ms; TE = 2.25 ms; flip angles (in degrees) = 3, 7, 12, 18, 25; matrix size = 64×128×128; field of view = 35×35×35 mm^3; scan time = 4:54 min:sec per flip angle.

Additionally, an actual flip-angle imaging (AFI) SPGR scan was acquired for flip angle mapping using the following parameters: TR1/TR2 = 5.9/29.5 ms; TE = 2.22 ms; flip angle = 55°; matrix size = 64×64×64; field of view = 35×35×35 mm^3 (41). R_1 times were estimated using weighted linear least squares estimation with flip angle correction (42). Images were acquired and R_1 maps were calculated pre-contrast and at days 1, 2, 4, 7, and 14 following $MnCl_2$ administration in order to analyze the *in vivo* dynamics of Mn^{2+} uptake and efflux.

To measure and quantify Mn^{2+} uptake in the whole brain and individual brain regions, brains were manually segmented from surrounding tissue at all imaging time points. Using FMRIB's Linear Image Registration Tool, FLIRT, manually segmented images were registered to a Waxholm Space atlas of the Sprague Dawley rat brain (43–47). Following registration, the atlas was used to segment the following sub-regions for further quantification and analysis: striatum, neocortex, olfactory bulb, corpus callosum, basal forebrain, globus pallidus, thalamus, hippocampus, hypothalamus, brain stem, cerebellum, and trigeminal tract. T_1 mapping, segmentation, registration, and image processing were performed in Matlab R2014b (The MathWorks, Natick, MA).

5.4. ^{52}Mn gamma counting of brain uptake

To observe the whole brain uptake of $^{52}Mn^{2+}$ following administration of NCA and CA $^{52}Mn^{2+}$, subjects were sacrificed either 24 hours (N=3 per contrast agent group) or 48 hours (N=3 per contrast agent group) following intravenous infusion of $^{52}Mn^{2+}$. The brain was immediately excised and rinsed once in distilled water, the olfactory bulb (and trigeminal nerves, if still intact) were removed, and the brain mass was measured. Brain-average $^{52}Mn^{2+}$ uptake was measured by gamma counting using the average of three 2-minute counts with gating centered on the 744 keV gamma peak. Counting data was corrected for known gamma counter efficiency and decay-corrected to injection time to calculate the percent injected dose per gram (%ID/g) of brain tissue. A two-tailed Student's t-test was used to compare the brain uptake of $^{52}Mn^{2+}$ based on contrast agent form and measurement time point.

5.5. ^{52}Mn PET

In vivo ^{52}Mn PET/CT was performed in six subjects (N=5 with NCA $^{52}Mn^{2+}$, N=1 with CA $^{52}Mn^{2+}$) on a Siemens Inveon microPET/CT (Siemens Medical Solutions, Erlangen, Germany). PET acquisition time points varied between subjects, as an essential aspect of this experiment was to guide the design of a consistent ^{52}Mn PET imaging protocol. In the first PET/CT experiment, two subjects were administered 2 mCi/kg $^{52}Mn^{2+}$ (one CA, one NCA) and 30–60 minute full-body PET/CT scans were acquired 1, 2, 4, and 7 days later with a single static time frame. Additionally, the subject delivered NCA $^{52}Mn^{2+}$ in this experiment was scanned 2 hours following delivery. This scan time point was not feasible for the other subject due to the negative combined effects of isoflurane and bulk $MnCl_2$ immediately after delivery. In a second experiment, four subjects delivered 2 mCi/kg NCA $^{52}Mn^{2+}$ were scanned for 30–60 minutes at 0.5, 1.5, 3.5, 7.5, 24, 48, and 72 hours following contrast delivery. Two of these subjects were additionally scanned at 7 days following delivery. For all full-body PET scans, continuous bed motion with 5 passes was

used for PET acquisition due to the relative size of the rat compared to the PET scanner field of view.

For PET/CT reconstruction, attenuation maps were calculated using manual registration of full-body PET and CT images. Attenuation-corrected PET images were then reconstructed using a vendor-provided 2-dimensional ordered subset expectation maximization (OSEM) reconstruction algorithm. Scatter correction was not applied during reconstruction due to the tendency of this correction to reduce detectable signal in low-count brain imaging protocols, as has been observed in $^{15}O[H_2O]$ brain activation studies and was expected in this setting (48). For each subject and time point, the brain-average %ID/g was calculated by comparing the uptake in the manually delineated whole brain to the total delivered activity and normalizing by the mass of the brain, assuming tissue density equal to that of water.

5.6. ^{52}Mn Biodistribution

Biodistribution of $^{52}Mn^{2+}$ was measured with *ex vivo* organ gamma counting in order to examine the uptake of both NCA and CA $^{52}Mn^{2+}$ in major organs of the rat. $^{52}Mn^{2+}$ was prepared either at a concentration of 0.33 mCi/mL (12.2 MBq/mL) in saline (NCA) or at an activity concentration of 0.37 mCi/mL (13.7 MBq/mL) in 66.7 mM $MnCl_2$. A target injection dose of 100 uCi was delivered to rats ($N = 3$ per time point and per contrast agent formulation) via tail vein infusion at a rate of 2 mL/hr for an average of 8–10 minutes. For CA $^{52}Mn^{2+}$, the added carrier dose corresponded to approximately 4.5 mg/kg $MnCl_2$. Animals were sacrificed and organs were harvested at 4 or 48 hours following initiation of contrast delivery. For each organ, the sample was weighed and activity was measured by gamma counting with a PerkinElmer Wizard 2480 (Waltham, MA, USA) to calculate %ID/g. For statistical analysis, a two-tailed Student's t-test was used to compare the uptake of $^{52}Mn^{2+}$ at 4 and 48 hours and for the two contrast agent formulations.

Supplementary Material

Refer to Web version on PubMed Central for supplementary material.

Acknowledgments

The authors would like to acknowledge Justin Jeffery (University of Wisconsin-Madison) for his dedicated assistance with PET/CT acquisition and processing, along with Sam Hurley Ph.D. (FMRIB Centre, University of Oxford), and Cheng Guan Koay Ph.D. (Walter Reed National Military Medical Center, National Intrepid Center of Excellence), for contributing T_1 mapping acquisition and processing tools. We greatly appreciate the assistance of Patrick J Lao and Tobey J Betthauser in reviewing the manuscript. This project was supported in part by funding from the University of Wisconsin Institute for Clinical and Translational Research, as a Clinical and Translational Science Award (CTSA) site of the National Center for Advancing Translational Sciences (NCATS) grant UL1TR000427. We would also like to acknowledge other funding sources, including the NIH (R01NS091540 to M.S., T32 GM008349 to R.H., T32 CA009206 to S.A.G.), the ALS Association (15-IIP-201 to M.S.), and the University of Wisconsin Foundation.

References

1. Regge D, Cirillo S, Macera A, Galatola G. Mangafodipir trisodium: review of its use as an injectable contrast medium for magnetic resonance imaging. Rep Med Imaging. 2009; 2:55–68.
2. Massaad CA, Pautler RG. Manganese-enhanced magnetic resonance imaging (MEMRI). Methods Mol Biol. 2011; 711:145–174. [PubMed: 21279601]

3. Suero-Abreu GA, Praveen Raju G, Aristizabal O, Volkova E, Wojcinski A, Houston EJ, Pham D, Szulc KU, Colon D, Joyner AL, Turnbull DH. In vivo Mn-enhanced MRI for early tumor detection and growth rate analysis in a mouse medulloblastoma model. Neoplasia. 2014; 16(12):993–1006. [PubMed: 25499213]
4. Kim PJ, Mahmoudi M, Ge X, Matsuura Y, Toma I, Metzler S, Kooreman NG, Ramunas J, Holbrook C, McConnell MV, Blau H, Harnish P, Rulifson E, Yang PC. Direct evaluation of myocardial viability and stem cell engraftment demonstrates salvage of the injured myocardium. Circ Res. 2015; 116(7):e40–e50. [PubMed: 25654979]
5. Pan D, Caruthers SD, Senpan A, Schmieder AH, Wickline SA, Lanza GM. Revisiting an old friend: manganese-based MRI contrast agents. Wiley Interdiscip Rev Nanomed Nanobiotechnol. 2011; 3(2):162–173. [PubMed: 20860051]
6. Au C, Benedetto A, Aschner M. Manganese transport in eukaryotes: the role of DMT1. Neurotoxicology. 2008; 29(4):569–576. [PubMed: 18565586]
7. Nordhoy W, Anthonsen HW, Bruvold M, Jynge P, Krane J, Brurok H. Manganese ions as intracellular contrast agents: proton relaxation and calcium interactions in rat myocardium. NMR Biomed. 2003; 16(2):82–95. [PubMed: 12730949]
8. Bruvold M, Nordhoy W, Anthonsen HW, Brurok H, Jynge P. Manganese-calcium interactions with contrast media for cardiac magnetic resonance imaging: a study of manganese chloride supplemented with calcium gluconate in isolated Guinea pig hearts. Invest Radiol. 2005; 40(3):117–125. [PubMed: 15714086]
9. Silva AC, Lee JH, Aoki I, Koretsky AP. Manganese-enhanced magnetic resonance imaging (MEMRI): methodological and practical considerations. NMR Biomed. 2004; 17(8):532–543. [PubMed: 15617052]
10. Ni Y, Petre C, Bosmans H, Miao Y, Grant D, Baert AL, Marchal G. Comparison of manganese biodistribution and MR contrast enhancement in rats after intravenous injection of MnDPDP and MnCl2. Acta Radiol. 1997; 38(4 Pt 2):700–707. [PubMed: 9245965]
11. Topping GJ, Schaffer P, Hoehr C, Ruth TJ, Sossi V. Manganese-52 positron emission tomography tracer characterization and initial results in phantoms and in vivo. Med Phys. 2013; 40(4):042502. [PubMed: 23556918]
12. Lewis CM, Graves SA, Hernandez R, Valdovinos HF, Barnhart TE, Cai W, Meyerand ME, Nickles RJ, Suzuki M. (52)Mn Production for PET/MRI Tracking Of Human Stem Cells Expressing Divalent Metal Transporter 1 (DMT1). Theranostics. 2015; 5(3):227–239. [PubMed: 25553111]
13. Graves SA, Hernandez R, Fonslet J, England CG, Valdovinos HF, Ellison PA, Barnhart TE, Elema DR, Theuer CP, Cai W, Nickles RJ, Severin GW. Novel Preparation Methods of (52)Mn for ImmunoPET Imaging. Bioconjug Chem. 2015; 26(10):2118–2124. [PubMed: 26317429]
14. Wooten AL, Lewis BC, Lapi SE. Cross-sections for (p,x) reactions on natural chromium for the production of (52,52m,54)Mn radioisotopes. Appl Radiat Isot. 2015; 96:154–161. [PubMed: 25497324]
15. Daube ME, Nickles RJ. Development of myocardial perfusion tracers for positron emission tomography. Int J Nucl Med Biol. 1985; 12(4):303–314. [PubMed: 3878834]
16. Buchholz M, Spahn I, Coenen HH. Optimized separation procedure for production of no-carrier-added radiomanganese for positron emission tomography. Radiochimica Acta. 2015; 103(12):893–899.
17. Deri MA, Zeglis BM, Francesconi LC, Lewis JS. PET imaging with (8)(9)Zr: from radiochemistry to the clinic. Nucl Med Biol. 2013; 40(1):3–14. [PubMed: 22998840]
18. Shokeen M, Wadas TJ. The development of copper radiopharmaceuticals for imaging and therapy. Med Chem. 2011; 7(5):413–429. [PubMed: 21711219]
19. Torigian DA, Zaidi H, Kwee TC, Saboury B, Udupa JK, Cho ZH, Alavi A. PET/MR imaging: technical aspects and potential clinical applications. Radiology. 2013; 267(1):26–44. [PubMed: 23525716]
20. Bade AN, Zhou B, McMillan J, Narayanasamy P, Veerubhotla R, Gendelman HE, Boska MD, Liu Y. Potential of N-acetylated-para-aminosalicylic acid to accelerate manganese enhancement decline for long-term MEMRI in rodent brain. J Neurosci Methods. 2015; 251:92–98. [PubMed: 26004847]

21. Liu CH, D'Arceuil HE, de Crespigny AJ. Direct CSF injection of MnCl(2) for dynamic manganese-enhanced MRI. Magn Reson Med. 2004; 51(5):978–987. [PubMed: 15122680]
22. Canals S, Beyerlein M, Keller AL, Murayama Y, Logothetis NK. Magnetic resonance imaging of cortical connectivity in vivo. Neuroimage. 2008; 40(2):458–472. [PubMed: 18222710]
23. Lee JH, Silva AC, Merkle H, Koretsky AP. Manganese-enhanced magnetic resonance imaging of mouse brain after systemic administration of MnCl2: dose-dependent and temporal evolution of T1 contrast. Magn Reson Med. 2005; 53(3):640–648. [PubMed: 15723400]
24. Chuang KH, Koretsky AP, Sotak CH. Temporal changes in the T1 and T2 relaxation rates (DeltaR1 and DeltaR2) in the rat brain are consistent with the tissue-clearance rates of elemental manganese. Magn Reson Med. 2009; 61(6):1528–1532. [PubMed: 19353652]
25. Crossgrove JS, Allen DD, Bukaveckas BL, Rhineheimer SS, Yokel RA. Manganese distribution across the blood-brain barrier. I. Evidence for carrier-mediated influx of managanese citrate as well as manganese and manganese transferrin. Neurotoxicology. 2003; 24(1):3–13. [PubMed: 12564377]
26. Aschner M. The transport of manganese across the blood-brain barrier. Neurotoxicology. 2006; 27(3):311–314. [PubMed: 16460806]
27. Yokel RA. Manganese flux across the blood-brain barrier. Neuromolecular Med. 2009; 11(4):297–310. [PubMed: 19902387]
28. Murphy VA, Wadhwani KC, Smith QR, Rapoport SI. Saturable transport of manganese(II) across the rat blood-brain barrier. J Neurochem. 1991; 57(3):948–954. [PubMed: 1861159]
29. Crossgrove J, Zheng W. Manganese toxicity upon overexposure. NMR Biomed. 2004; 17(8):544–553. [PubMed: 15617053]
30. Eschenko O, Canals S, Simanova I, Logothetis NK. Behavioral, electrophysiological and histopathological consequences of systemic manganese administration in MEMRI. Magn Reson Imaging. 2010; 28(8):1165–1174. [PubMed: 20096525]
31. Aoki I, Wu YJ, Silva AC, Lynch RM, Koretsky AP. In vivo detection of neuroarchitecture in the rodent brain using manganese-enhanced MRI. Neuroimage. 2004; 22(3):1046–1059. [PubMed: 15219577]
32. Takeda A, Sawashita J, Okada S. Biological half-lives of zinc and manganese in rat brain. Brain Res. 1995; 695(1):53–58. [PubMed: 8574647]
33. Zofkova I, Nemcikova P, Matucha P. Trace elements and bone health. Clin Chem Lab Med. 2013; 51(8):1555–1561. [PubMed: 23509220]
34. Gavin CE, Gunter KK, Gunter TE. Mn2+ sequestration by mitochondria and inhibition of oxidative phosphorylation. Toxicol Appl Pharmacol. 1992; 115(1):1–5. [PubMed: 1631887]
35. Van Baelen K, Dode L, Vanoevelen J, Callewaert G, De Smedt H, Missiaen L, Parys JB, Raeymaekers L, Wuytack F. The Ca2+/Mn2+ pumps in the Golgi apparatus. Biochim Biophys Acta. 2004; 1742(1–3):103–112. [PubMed: 15590060]
36. Ambudkar IS. Regulation of calcium in salivary gland secretion. Crit Rev Oral Biol Med. 2000; 11(1):4–25. [PubMed: 10682899]
37. Aschner M, Gannon M, Kimelberg HK. Manganese uptake and efflux in cultured rat astrocytes. J Neurochem. 1992; 58(2):730–735. [PubMed: 1729413]
38. Seshadri M, Hoy A. Manganese-enhanced MRI of salivary glands and head and neck tumors in living subjects. Magn Reson Med. 2010; 64(3):902–906. [PubMed: 20806380]
39. Malaisse WJ, Maedler K. Imaging of the beta-cells of the islets of Langerhans. Diabetes Res Clin Pract. 2012; 98(1):11–18. [PubMed: 22854107]
40. Rief M, Huppertz A, Asbach P, Franiel T, Schwenke C, Hamm B, Taupitz M, Wagner M. Manganese-based oral contrast agent for liver magnetic resonance imaging: evaluation of the time course and dose response of liver signal intensity enhancement. Invest Radiol. 2010; 45(9):565–571. [PubMed: 20644484]
41. Yarnykh VL. Actual flip-angle imaging in the pulsed steady state: a method for rapid three-dimensional mapping of the transmitted radiofrequency field. Magn Reson Med. 2007; 57(1):192–200. [PubMed: 17191242]
42. Chang LC, Koay CG, Basser PJ, Pierpaoli C. Linear least-squares method for unbiased estimation of T1 from SPGR signals. Magn Reson Med. 2008; 60(2):496–501. [PubMed: 18666108]

43. Jenkinson M, Smith S. A global optimisation method for robust affine registration of brain images. Med Image Anal. 2001; 5(2):143–156. [PubMed: 11516708]

44. Jenkinson M, Bannister P, Brady M, Smith S. Improved optimization for the robust and accurate linear registration and motion correction of brain images. Neuroimage. 2002; 17(2):825–841. [PubMed: 12377157]

45. Papp EA, Leergaard TB, Calabrese E, Johnson GA, Bjaalie JG. Waxholm Space atlas of the Sprague Dawley rat brain. Neuroimage. 2014; 97:374–386. [PubMed: 24726336]

46. Kjonigsen LJ, Lillehaug S, Bjaalie JG, Witter MP, Leergaard TB. Waxholm Space atlas of the rat brain hippocampal region: three-dimensional delineations based on magnetic resonance and diffusion tensor imaging. Neuroimage. 2015; 108:441–449. [PubMed: 25585022]

47. Sergejeva M, Papp EA, Bakker R, Gaudnek MA, Okamura-Oho Y, Boline J, Bjaalie JG, Hess A. Anatomical landmarks for registration of experimental image data to volumetric rodent brain atlasing templates. J Neurosci Methods. 2015; 240:161–169. [PubMed: 25445058]

48. Zaidi H, Koral KF. Scatter modelling and compensation in emission tomography. Eur J Nucl Med Mol Imaging. 2004; 31(5):761–782. [PubMed: 15057488]

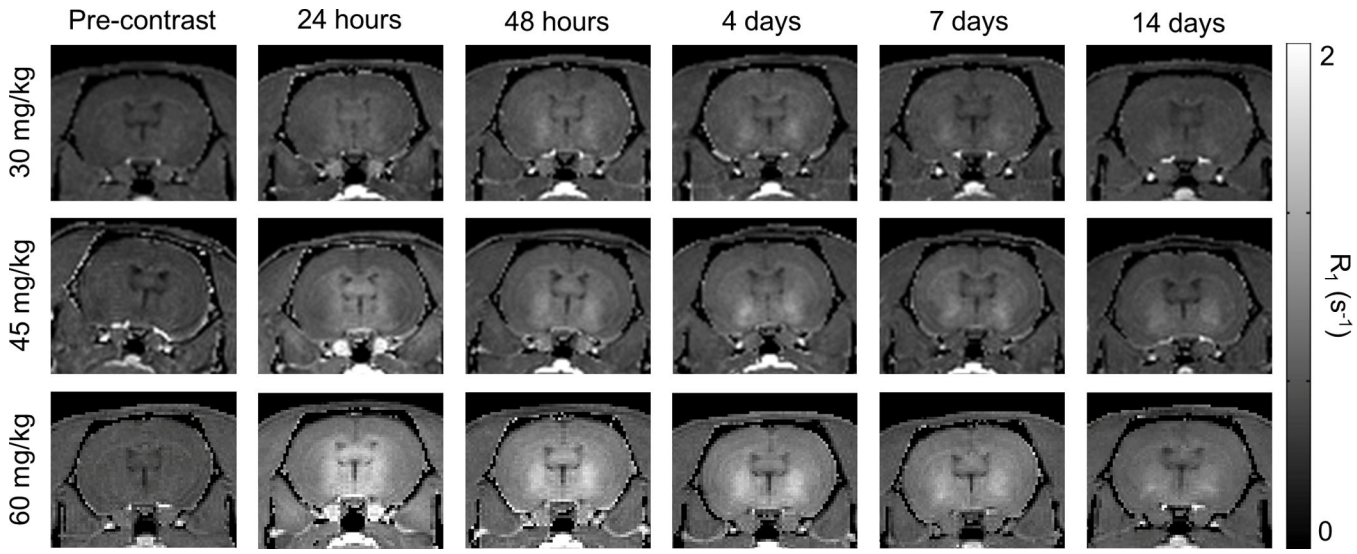

Figure 1.

Representative coronal R_1 maps of three subjects delivered different doses of $MnCl_2$ (30, 45, and 60 mg/kg). Imaging was performed and R_1 maps were calculated prior to contrast administration and at five imaging time points over two weeks following administration. Higher contrast dose increases signal enhancement, particularly near the ventricles. Two weeks following contrast administration, signal enhancement remains, particularly in the vicinity of the striatum and globus pallidus.

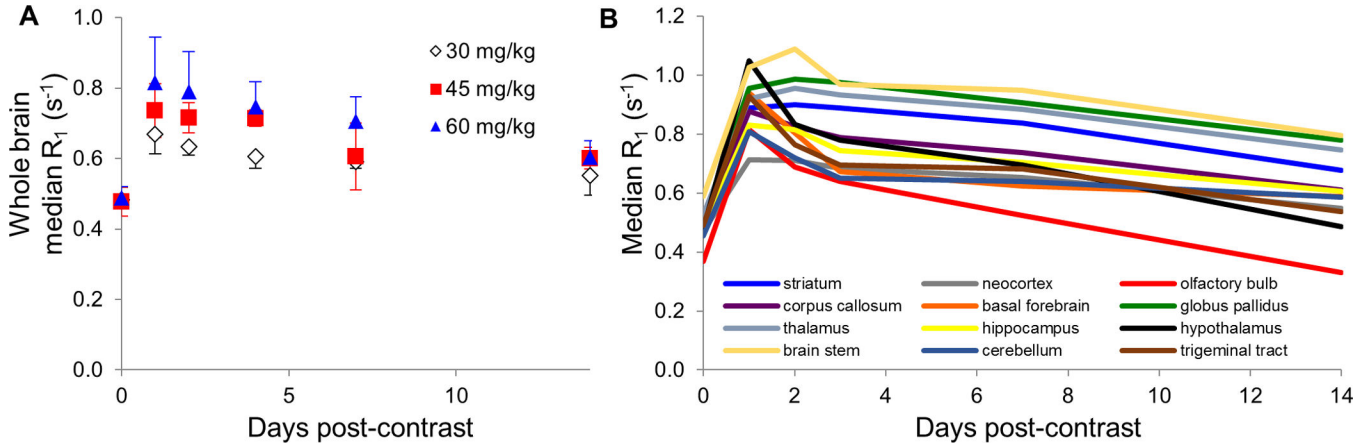

Figure 2.

Uptake of Mn in the whole brain and various brain regions measured with quantitative MRI. (A) Whole-brain average R_1 relaxation rate reached a maximum 24 hours following contrast administration regardless of contrast dose ranging from 30–60 mg/kg $MnCl_2$. Efflux from the brain was slow, with some enhancement remaining at the 14 day imaging time point. (B) Regional analysis of uptake of 60 mg/kg $MnCl_2$ based on registration and segmentation of brain volumes to a rat brain atlas. Some brain regions (neocortex, corpus callosum, basal forebrain, hippocampus, hypothalamus, and cerebellum) reached maximum enhancement one day following contrast administration, while others (striatum, globus pallidus, thalamus, and brain stem) in some cases reached maximum at two or four days post-contrast.

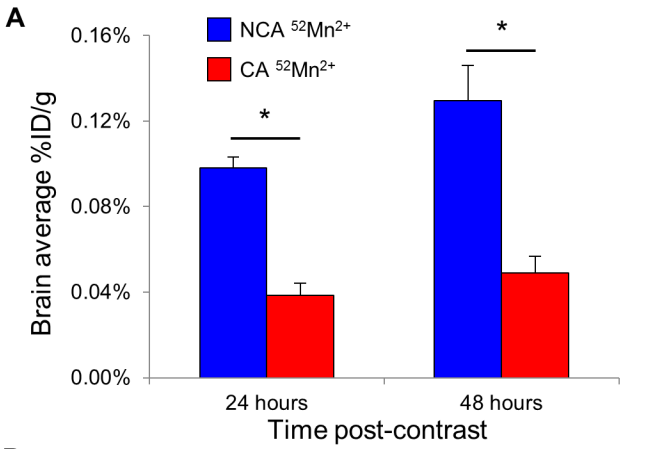

B

Brain average $^{52}Mn^{2+}$ uptake	Average %ID/g		% increase 24 vs. 48 hr
	24 hr	48 hr	
CA $^{52}Mn^{2+}$	0.039	0.049	27.3%
NCA $^{52}Mn^{2+}$	0.098	0.130	32.1%
% increase NCA vs. CA	254% *	264% *	*p<0.01

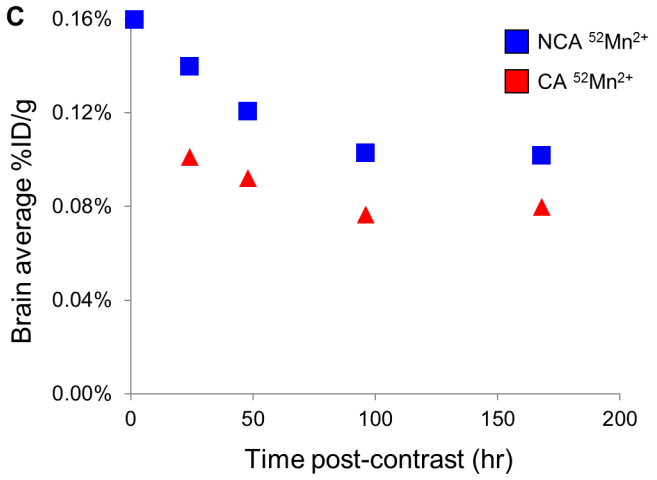

Figure 3.

Comparison of brain uptake of no-carrier-added (NCA) and carrier-added (CA) ^{52}Mn with *ex vivo* gamma counting and *in vivo* PET/CT. We observed higher activity uptake of NCA ^{52}Mn in both *ex vivo* gamma counting measurements of the excised brain at 24 and 48 hours (A, B) as well as *in vivo* with PET/CT for up to 7 days following contrast delivery (C). *Ex vivo* measurements are the average of 3 subjects per contrast agent formulation and time point, while *in vivo* PET/CT was performed on one subject per contrast agent formulation in this initial comparative imaging study.

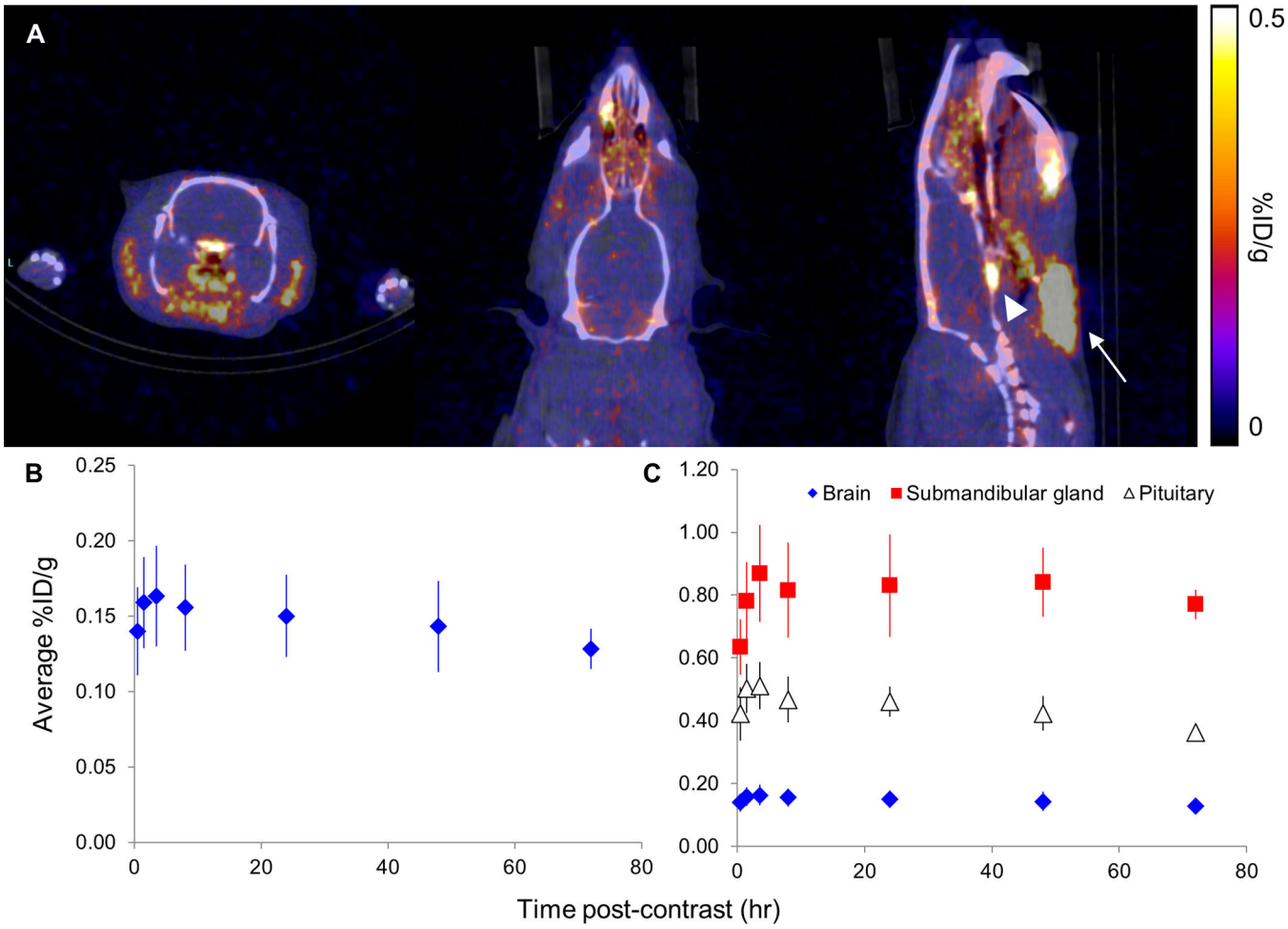

Figure 4.

In vivo PET/CT of brain uptake of NCA ^{52}Mn in the rat. (A) Coronal, axial, and sagittal views of the brain (left to right, respectively) from *in vivo* PET/CT of a rat four hours following administration of no-carrier-added (NCA) ^{52}Mn. Submandibular gland = white arrow, pituitary = white arrowhead. (B) In four subjects, average brain uptake reached a maximum at four hours following contrast administration, after which a slow decrease in brain signal was observed. (C) High ^{52}Mn uptake in the submandibular gland and pituitary, up to 0.869 and 0.512 %ID/g respectively, were measured at all imaging time points.

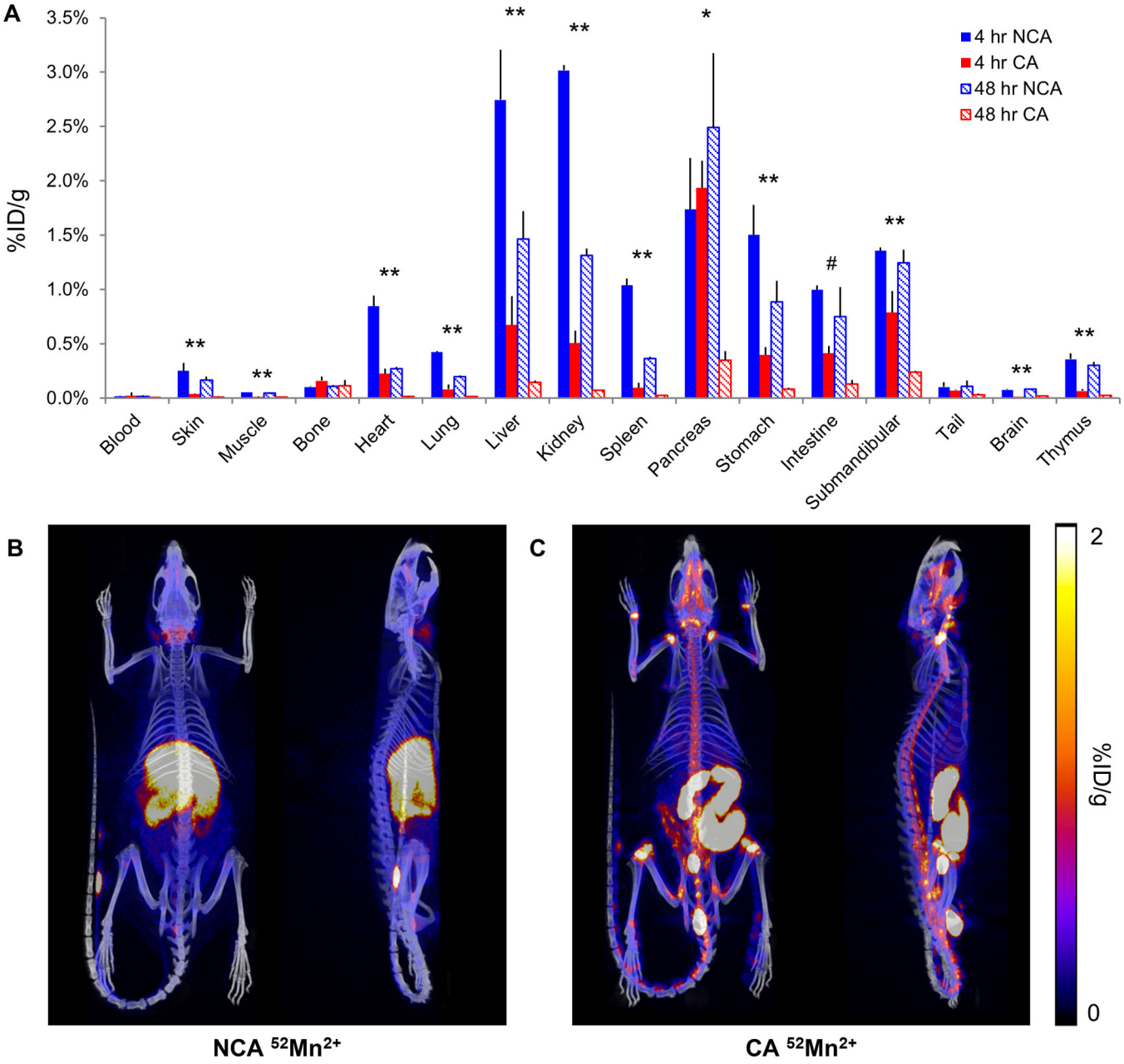

Figure 5.

Biodistribution of no-carrier-added (NCA) and carrier-added (CA) ^{52}Mn in the rat. (A) *Ex vivo* biodistribution of NCA and CA ^{52}Mn in the rat at 4 and 48 hours following administration; N=3 per contrast agent preparation and time point. A significant increase in uptake of NCA ^{52}Mn compared to CA ^{52}Mn was observed at both time points in the majority of organs tested (**p<0.05). In the pancreas and intestine, this increase was only significant at one time point (*p<0.05 at four hours, $^{\#}p$<0.05 at 48 hours). No significant differences were observed in the blood, bone, or tail. (B–C) Representative PET/CT overlay MIPs of full-body ^{52}Mn uptake at 24 hours following contrast delivery from one subject per contrast agent formulation. (B) In the NCA subject, uptake is observed in the submandibular

glands, nasal cavities, liver, kidneys, intestine, pancreas, and spleen. (C) In the CA subject, the majority of uptake is observed in the contents of the intestine and in the vicinity of the intervertebral and synovial joints.

Table 1

Maximum R_1 relaxation rate (s^{-1}) reached by brain region and $MnCl_2$ dose delivered, along with corresponding percent increase in R_1 with respect to the pre-contrast measurement. Entries are color-coded by the imaging time point at which the maximum signal was reached; red = 24 hours, blue = 48 hours, green = 96 hours (4 days). No regions reached their maximum after the 96 hour imaging time point.

$MnCl_2$ Dose	Striatum		Neocortex		Olfactory bulb		Corpus callosum		Basal forebrain		Globus pallidus	
30 mg/kg	0.711	41%	0.611	33%	0.685	54%	0.698	42%	0.697	40%	0.743	39%
45 mg/kg	0.825	70%	0.656	43%	0.736	76%	0.766	58%	0.851	65%	0.904	72%
60 mg/kg	0.899	84%	0.713	52%	0.815	121%	0.878	77%	0.939	85%	0.987	92%
	Thalamus		Hippocampus		Hypothalamus		Brain stem		Cerebellum		Trigeminal tract	
30 mg/kg	0.747	37%	0.702	49%	0.814	48%	0.8	41%	0.635	37%	0.659	48%
45 mg/kg	0.871	67%	0.768	65%	0.99	91%	0.911	59%	0.693	51%	0.732	53%
60 mg/kg	0.956	82%	0.83	74%	1.049	120%	1.088	85%	0.809	78%	0.929	90%